PNAS

Supporting Information for

Variable carbon isotope fractionation of photosynthetic communities over depth in an open-ocean euphotic zone

Lillian C. Henderson, Fabian Wittmers, Craig A. Carlson, Alexandra Z. Worden, Hilary G. Close

Corresponding author: Lillian C. Henderson

Email: lillian.henderson@earth.miami.edu

This PDF file includes:

Supporting Information Text

SI 1. Supplemental information about the phytol analysis method. As described in the main text, we separated extracted lipids into three compound class fractions in order to isolate the photosynthetic signal via the $\delta^{13}C$ value of phytol from intact chlorophyll (polar lipid fraction). We also collected a sterol fraction and an alcohol fraction. This approach is in contrast to other studies that have analyzed total phytol in particulate samples [e.g., (1)]. We analyzed all three compound class fractions and recovered phytol cleaved from the polar lipid fraction in all samples from the surface 200 m of the water column (Table S1). In some cases, a small amount of polar lipids was also captured in the sterol fraction (Table S1; Figure 1a). Free phytol concentrations were below the limits of quantitation or detection in all samples and all compound class fractions (Table S1); thus, the separation step proved unnecessary for our euphotic zone samples but could be useful for future studies of sinking particles or sediments, where detrital contributions may be more important.

We measured phytol concentrations via gas chromatography coupled to a mass spectrometer (GC-MS); yields aligned well with those from GC-IRMS (adjusted R^2=0.91, $p<0.0001$, slope = 1.08; Figure S13). Further, both GC-MS and GC-IRMS results were similar to *in-vivo* chlorophyll fluorescence except for one outlier at 120 m (adjusted R^2=0.58, $p<0.05$, slope = 0.88, outlier omitted), supporting the cleavage of our measured phytol from chlorophyll rather than other structures (Figure S14). The outlier sample at 120 m measured chlorophyll concentrations higher than those from *in vivo* fluorescence but also had greater uncertainty in the sampling depth than other samples (±8 m; Table S1), potentially explaining the discrepancy. Alternatively, a high concentration of chlorophyll *b* in the LEZ may be responsible for higher concentrations of phytol recovered compared to predictions from chlorophyll fluorescence. Chlorophyll *b* was present in a ratio of almost 1:1 with chlorophyll *a* at these depths in the BATS time-series data set (http://bats.bios.edu/bats-data/). Chlorophyll *b* would contribute to phytol cleaved from intact polar lipids that we measured yet is likely underrepresented in estimates of chlorophyll via *in vivo* fluorescence, as the two have different but overlapping emission spectra (2). Regardless, chlorophylls *a* and *b* are known to have similar carbon isotope composition within the same organism (3).

Prior studies have established that the proportion of total pigments comprised of phaeopigments such as phaeophytin increases over depth within the euphotic zone (4, 5). Phaeophytin may also be captured but perhaps underrepresented in estimates of chlorophyll from *in vivo* fluorescence. However, phaeophytin is converted back into chlorophyll when living cells are exposed to light after being in the dark (4), suggesting that phaeophytin is stored in viable phytoplankton cells rather than in detrital material. Thus, presence/absence of phaeophytin does not change the interpretation of our $\delta^{13}C_{phytol}$ data. Furthermore, while phytol can also be included as a side chain in some zooplankton lipids [wax esters; (6)], our measurements would not include these sources because we analyzed the polar lipid fraction and focused only on the 0.3-6 µm particles, a size fraction that would exclude most zooplankton contribution. Our analysis of larger particle fractions (>20 µm), which would capture intact fecal pellets, show no difference in $\delta^{13}C_{POC}$ values from the surface to the LEZ (Figure S15).

SI 2. Phytoplankton cell counts and estimates of phytoplankton biomass concentrations, growth rates, and $\delta^{13}C$ values

SI 2.1 Estimates of phytoplankton biomass $\delta^{13}C$ values and assessing uncertainty around phytol as a proxy for phytoplankton biomass. 1.2-6 µm phytoplankton biomass $\delta^{13}C$ values were calculated using Equation 1 with an offset of total phytoplankton biomass minus phytol

($\Delta\delta^{13}C_{p\text{-}phytol}$) of 3.5‰ throughout the euphotic zone, as this is the calculated average offset from recently compiled culture data [3.5±1.3‰; (7)].

To assess the uncertainty associated with potential variability in the average offset ($\Delta\delta^{13}C_{p\text{-}phytol}$) over depth within the euphotic zone, phytoplankton biomass $\delta^{13}C$ values were calculated with a variable offset throughout the euphotic zone (Figure S4). The two variations tested were:

1) an offset of total phytoplankton biomass minus phytol of 2.2‰ at 0-90 m and 4.8‰ at 90-120 m; values are the average offset plus/minus 1 standard deviation (3.5±1.3‰)
2) an offset of total phytoplankton biomass minus phytol of 4.8‰ at 0-90 m and 2.2‰ at 90-120 m; values are also the average offset plus/minus 1 standard deviation (3.5±1.3‰)

We also considered the possibility that the $\delta^{13}C$ value of most phytoplankton biomass remains constant throughout the euphotic zone while only the $\delta^{13}C$ value of chlorophyll changes by the magnitude of our measured $\delta^{13}C_{phytol}$ values; we found that phytoplankton biomass $\delta^{13}C$ values would decrease by <0.4‰ from 30 to 120 m, suggesting that variations in chlorophyll $\delta^{13}C$ values and concentrations alone cannot account for the variation in $\delta^{13}C_{POC}$ values. We estimate that chlorophyll makes up 0.8-4.7% of total phytoplankton carbon and only 0.16-1.6% of total POC in the euphotic zone at this site, further indicating that changes in only the $\delta^{13}C$ value of chlorophyll would be insufficient to cause the observed $\delta^{13}C_{POC}$ difference of 2.7‰ over depth.

SI 2.2 Sampling and processing for flow cytometry. Samples for phytoplankton cell enumeration were collected during the July 2018 cruise (AE18-19). Water was collected in a small bottle from the Niskin, and then 3 mL were aliquoted into a 15 mL conical tube. Samples were fixed to a final concentration of 1% EM grade glutaraldehyde, briefly vortexed, and incubated for 20 min in the dark before being flash-frozen in liquid nitrogen. Samples were then stored at -80°C. Samples were analyzed using a BD Influx Flow Cytometer with a 100 mW 488 nm laser colinear with a 200 mW 457 nm laser and forward angle light scatter (FALS) used as the trigger (BD Biosciences). Phototrophs were identified by red chlorophyll autofluorescence (692/40 nm bandpass) vs FALS or orange phycoerythrin autofluorescence vs FALS. Three general groups were resolved, *Prochlorococcus*, *Synechococcus*, and eukaryotes.

SI 2.3 Estimates of phytoplankton biomass and specific growth rates. Total phytoplankton community biomass as a proportion of total POC was estimated in four ways: [1] phytoplankton carbon was calculated by multiplying C:chl ratios, which varied with light intensity (depth) according to (8, 9), and chlorophyll concentrations determined by measured CTD fluorescence. A Monte Carlo method was used to propagate uncertainty in the fluorescence profiles throughout the cruise and C:chl ratio calculations. The total POC concentration was calculated rather than measured directly: POC concentration in the 1.2-6 µm size fraction was measured, and the proportion of total POM the 1.2-6 µm size fraction made up on average (69±5%) was estimated from measurement of particulate carbon concentrations in all particle size classes (0.3-1.2 µm, 1.2-6 µm, 6-20 µm, >20 µm). [2] Biomass carbon in three phytoplankton groups (*Prochlorococcus*, *Synechococcus*, and small eukaryotes) was calculated using flow cytometry cell abundances, average cell diameters over depth (10), and biovolume to cellular carbon calculations (11). A Monte Carlo method was used to account for uncertainty in average cell diameters and biovolume:C calculations. [3] Same as [2], but calculated specifically for the 1.2-6 µm size fraction. [4] Same as [3], but utilizing biovolume to biomass conversions in Worden

et al. 2004. All eukaryotes were assumed to be captured in this size fraction, and for *Prochloroccus* and *Synechococcus*, 40-80% of the measured cell abundances were included in the calculation, to account for the proportion of cyanobacteria captured in the 1.2-6 µm size fraction, as opposed to having gone through the 1.2 µm pore-size filter for collection on the 0.3 µm filter. The proportion of cyanobacteria retained on the 1.2 µm filter was estimated in two ways from [1] measured chlorophyll concentrations in the 0.3-1.2 and 1.2-6 µm size fractions and [2] the ratio of *Pelagomonas* to *Prochlorococcus* 16S rRNA gene ASVs in each size fraction, with the supportable assumption that all *Pelagomonas* cells were retained on the 1.2 µm filter. While cyanobacteria are typically smaller in diameter than 1.2 µm, the pore size of filters is known to decrease when heavily loaded (12), moreover average FALS (a size-related proxy) of the *Prochlorococcus* community in our study increased by 4-fold between the surface and deeper regions of the photic zone; finally, capture of cyanobacteria in this size fraction is evident in 16S amplicon results. Calculated phytoplankton carbon in the 1.2-6 µm size fraction was then divided by the measured POC concentration in the 1.2-6 µm size fraction. A Monte Carlo method was used to account for uncertainty in average cell diameters, biovolume to biomass C calculations, and the proportion of cyanobacteria cells captured in the 1.2-6 µm size fraction. [4] Same as [3], but using a biovolume to cellular carbon conversion of 237 fg C μm^{-3} (13) with no uncertainty on this number included in the Monte Carlo method. Average cell diameters and surface area to volume ratios (SA/V) were calculated from measured cellular abundances (SI 2.2) and previously measured cell diameters (10).

Average growth rates for the total phytoplankton community were estimated by dividing net primary production by calculated phytoplankton biomass. We used biomass estimated from cell abundances for total seawater (estimate 2 above) and net primary production data averaged from BATS cruises in June and July 2018-2019.

SI 2.4 Adjustment of data for photosynthetic carbon isotope fractionation diffusional model. Calculated ε_p values, growth rates, and effective surface area to volume ratios of 1.2-6 µm phytoplankton (total surface area divided by total biovolume) were used to compare our environmental data to that of culture data in the context of diffusional models of photosynthetic carbon isotope fractionation (14–16). Placement of environmental data in this context must account for differences in the growth period used in cultures versus the natural environment, as many cultures are grown under continuous light conditions. Laws et al. (14) multiplied growth rates by a factor of 2.35 to calculate instantaneous growth rates during the photoperiod and account for respiration effects, while other studies used 24 hour growth rates (17, 18). For consistency, all environmental growth rates, including our own, were adjusted to account for daylength as suggested by Laws et al. (14) using daylengths calculated from approximate latitudes via the NOAA Solar Calculator (available online: https://gml.noaa.gov/grad/solcalc/).

SI 2.5 Estimation of non-phytoplankton biomass POC $\delta^{13}C$ values. The $\delta^{13}C$ value of other POC (non-phytoplankton biomass) was calculated using a mass balance calculation with concentrations and $\delta^{13}C$ values of phytoplankton biomass and total POC:

$$\delta^{13}C_{other} = \frac{\delta^{13}C_{POC} * C_{POC} - \delta^{13}C_p * C_p}{C_{other}} \quad \text{(S1)}$$

where $\delta^{13}C_p$ is the $\delta^{13}C$ value of phytoplankton biomass, C_p represents the concentration of phytoplankton biomass, $\delta^{13}C_{other}$ is the $\delta^{13}C$ value of non-phytoplankton POC, and C_{other} is the concentration of non-phytoplankton POC. $\delta^{13}C_{POC}$ and C_{POC} were measured via EA-IRMS (see

Materials and Methods), $\delta^{13}C_p$ was calculated as in Equation 1, C_p was calculated via the biomass calculations in SI 2.3, and C_{other} was calculated as the difference between C_{POC} and C_p.

SI 3. Collection and processing of samples for whole seawater and size-fractionated particle amplicon sequencing

SI 3.1 Size-fractionated DNA extraction from filters. DNA was extracted by first thawing bags and adding 6 ml of sucrose lysis buffer (40 mmol/L EDTA, 50 mmol/LTris HCl, 750 mmol/L sucrose, 400 mmol/L NaCl, pH adjusted to 8.0), 600 µl of sodium dodecyl sulfate (10% w/v) and 10 µl of 20 mg/mL proteinase K to the bag. Bags were resealed and incubated at 37°C for 30 min and then increased to 55°C for another 30 min. Approximately 1.1 ml of lysate was removed by sterile serological pipet to 2 mL tubes and the remaining lysate was stored at -80°C. DNA was extracted from the lysate following the phenol and chloroform protocol of (19) and quantified at the University of California Santa Barbara.

SI 3.2 Amplicon library sequencing & bioinformatics for size-fractionated DNA. Amplification of the V4 region of the 16S rRNA gene was performed using the 515F-Y (5'-GTGYCAGCMGCCGCGGTAA-3') and 806RB (5'-GGACTACNVGGGTWTCTAAT-3') primers with custom adapters (20–22). The 806RB primer does not amplify *Mamiellophyceae* 16S rRNA (23), but this bias had no major influence on the interpretation of data given the minor abundance of *Mamiellophyceae* detected in the whole community analysis during the time of sampling (SI 1.4). PCR-grade water process blanks and mock communities (BEI Resources mock communities HM-782D and HM-783D) were included with each 96-well plate of samples as quality control checks. Amplicons were cleaned and normalized using SequalPrep plates (Invitrogen), pooled at equal volumes, concentrated using Amicon Ultra 0.5 ml centrifugal tubes (Millipore), gel extracted using the QIAquick Gel Extraction Kit to remove non-target DNA (Qiagen) and sequenced on an Illumina MiSeq using PE250 chemistry at University of California (UC), Davis DNA Technologies Core.

Samples were demultiplexed at UC Davis DNA Technologies Core. FastQ files were quality filtered and merged using the dada2 package (version 1.22) in R (24). Chimeras were removed de novo using the removeBimeraDenovo function in the dada2 package. Forward reads were trimmed to 230bp, reverse reads were trimmed to 160bp in dada2. Amplicon sequence variants (ASVs) were given a taxonomic assignment in the dada2 package using the assignTaxonomy command and the SILVA database [version 138.1 with species; (25)]. For finer phylogenetic taxonomy assignment of SAR11, SAR202, and cyanobacterial clades, sequences were further run through a modified version of PhyloAssigner [(26); available through https://github.com/BIOS-SCOPE/PhyloAssigner_python_UCSB] using specialized clade-specific reference databases for SAR11 (27), SAR202 (28), and cyanobacteria (29). Samples were rarefied to 8000 reads, and samples with fewer than 8000 reads were removed from further analysis, which amounted to 25 out of 478 environmental samples. Sequences identified as plastid sequences using SILVA v138.1 were re-classified in qiime2 (v2020.11) using scikit (v0.23.1) with a trained classifier for the 16S plastid fraction of the PR2 database (11; v14.4) trimmed to the V4 region. Mock communities and negative controls were checked to confirm consistency in amplification and lack of contamination between PCR plates and then removed from further analysis. DNA sequence data are available in the National Center for Biotechnology Information (NCBI) Sequence Read Archive (SRA) under project number PRJNA769790.

SI 3.3 Sample collection for whole-seawater DNA sequencing. Seawater was collected from up to 10 depths within the upper 500 m by 12 L Niskin-type sampling bottles (Ocean Test Equipment Inc.). 4 L of seawater per depth were filtered using 0.2 µm Sterivex filters (polyethersulfone membrane, Millipore, Burlington, MA, United States). Samples were stored in sucrose lysis buffer at -80°C until extraction using a phenol-chloroform protocol (19).

SI 3.4 16S rRNA Gene V1-V2 Amplicon PCR and Sequencing for whole seawater DNA. PCR to amplify the V1-V2 region of the 16S ribosomal RNA (rRNA) gene was conducted using the primers 27F and 338R with general Illumina overhang adapters (26, 31). Libraries were pooled to equimolar concentration and sequenced using a single 2x 250 paired-end lane with MiSeq Reagent Kit v2 at the Center for Biocomputing (Oregon State University), Corvallis, Oregon. Sequences were trimmed and processed to amplicon sequence variants (ASVs) using the DADA2 R package v1.14 (24) with trimming cutoffs 180 for forward and 150 for reverse reads. Chimeric sequences were removed within the dada2 pipeline using default settings.

SI 3.5 Amplicon Phylogenetic Placement for whole seawater DNA. 16S rRNA V1-2 representative ASVs were processed using a modified version of PhyloAssigner (26) available through https://github.com/BIOS-SCOPE/PhyloAssigner_python_UCSB. Briefly, amplicons are aligned to an unmasked alignment based on full-length sequences and then placed on a phylogenetic tree using PPlacer (32). A global phylogenetic reference tree was used to identify potential Cyanobacteria and plastid reads. Reads assigned to those group were then taxonomically placed using a Cyanobacteria and plastid phylogeny with only Cyanobacteria being reclassified again using a designated Cyanobacteria phylogenetic tree (29). Stramenopile ASVs, and Pelagophytes and Dictyochophytes in particular were further classified using reference phylogenies as previously described (33).

SI 4. Seawater chemistry sampling, analysis, and calculations.

SI 4.1 Nutrient concentrations. Unfiltered seawater samples were collected in 20 mL HDPE vials during the July 2018 cruise (AE18-19). Samples were frozen at -20˚C, and analyzed using flow injection analysis on a QuickChem 8000 (Lachat Instruments, Zellweger Analytics, Inc.) by the University of California, Santa Barbara Marine Science Institute Analytical Laboratory (detection limits: NO_2^- + NO_3^-, 0.2 µmol/L; PO_4^{3-}, 0.1 µmol/L). Depth resolution was roughly every 20 m in the upper euphotic zone and every 40 m in the lower euphotic zone.

SI 4.2 Dissolved inorganic carbon system speciation and isotopes. Water samples for DIC and alkalinity concentrations were collected in both August and November 2021. Samples were collected with tubing directly from the Niskin into 250 mL glass screw-top bottles with Teflon tape on the threads. Sampling procedure followed that of the BATS protocol (34). Briefly, bottles were rinsed and overfilled at least one time with care taken to avoid air bubbles. A small headspace was left at the top of the bottle. Samples were preserved with 40 µL saturated mercuric chloride ($HgCl_2$), inverted to mix, and stored in the dark until processing. DIC and alkalinity samples were analyzed in the Marine Biogeochemistry Lab at BIOS (Nicholas Bates) using a VINDTA 3C.

Filter water samples for $\delta^{13}C_{DIC}$ were collected in both August and November 2021 using a plastic syringe equipped with a 3-way stopcock and a disposable 0.2 µm polyethersulfone filter. Sample bottles were rinsed with sample water, and water was filtered directly into acid-cleaned 40 mL glass serum bottles. Samples were preserved with 20 µL saturated $HgCl_2$ and sealed with a butyl

rubber septum and metal crimp, leaving minimal headspace. Samples were stored in the dark until processing. $\delta^{13}C_{DIC}$ samples were analyzed in the Stable Isotope Laboratory at University of Miami using a Gasbench coupled to a Thermo Delta V using methods identical to those used by Scranton et al. (35). Analytical uncertainty was ±0.2‰ as determined from analysis of standard solutions.

SI 4.3 Calculation of carbon dioxide concentration and carbon isotope composition.
Aqueous carbon dioxide concentrations were calculated using CO2SYS software for MATLAB, version 1.1 (36). Temperature and salinity data for the calculation were acquired from the CTD cast from which DIC samples were collected. SiO_2 and PO_4^{3-} data from the BATS bottle file from July/August and November 2018-2019 were used in the calculation for AE21-14 and AE21-23, respectively. K1/K2 dissociation constants used are those established in (37). K_{SO4} dissociation constant used was from (38) and the borate-to-salinity ratio used was from (39).

$\delta^{13}C_{CO2}$ values were calculated from measured $\delta^{13}C_{DIC}$ values and temperatures as in the following equation:

$$\delta^{13}C_{CO2} = \delta^{13}C_{DIC} + 23.644 - (9701.5/T_K)$$

where T_K is the seawater temperature in Kelvin (16, 40, 41).

SI 5. Extended Materials and Methods.

Particle samples for bulk POC carbon isotope analysis in additional seasons (Figure S3)

Small-volume (≤4 L) particle samples were collected according to BATS POC protocol (34) in August and November 2021 (AE21-14 and AE21-23). After collection, filters were folded in half with clean forceps, stored in combusted foil, and transported and stored at -80°C. Small-volume particle samples were processed and analyzed in the same way as large-volume pump samples except samples were not split; whole filters were prepared for analysis.

Extraction and purification of amino acids

Quantitative splits from 0.3 µm GF75 and 1.2 µm GF/C filters were freeze-dried, hydrolyzed, purified, derivatized, and analyzed for nitrogen and carbon isotope composition of individual amino acids as in Hannides et al. (42), Doherty et al. (43), and Wojtal et al. (44). Briefly, size-fractionated filter splits were hydrolyzed (20 h, 110°C) using trace metal grade 6 N hydrochloric acid. Amino acids were then purified via 5 cm cation exchange columns (50W-X8 analytical grade resin, 100-200 mesh) (45) and then converted to trifluoroacetyl isopropyl ester derivatives for analysis. Filter splits for carbon and nitrogen isotope analysis of individual amino acids contained between 28-127 L and 46-70 L for 1.2 µm GF/C and 0.3 µm GF75 filters, respectively.

Carbon and nitrogen isotope analysis of amino acids

Derivatized amino acids were analyzed for carbon and nitrogen isotope composition via GC-IRMS using a BPX5 column (50 m x 0.32 mm, 1.0 µm film thickness; SGE Analytical Science, Trajan Scientific and Medical); methods were identical to those reported in Doherty et al. (43) and Wojtal et al. (44). Samples were analyzed with duplicate or triplicate injections. A standard mixture of 14 amino acids with known $\delta^{13}C$ and $\delta^{15}N$ values was prepared alongside as samples and was used

to correct for instrument drift and any potential peak size relationships, as well as carbon added during derivatization in the case of $\delta^{13}C$ values. Norleucine and aminoadipic acid standards with known $\delta^{13}C$ and $\delta^{15}N$ values were coinjected with both the standard mixture and samples. Error was propagated in the same way as for the phytol samples and includes [1] uncertainty in the standard $\delta^{13}C$ value, [2] the replicate variability of the standard, and [3] the replicate variability of the sample. $\delta^{15}N$ values were calculated relative to atmospheric N_2.

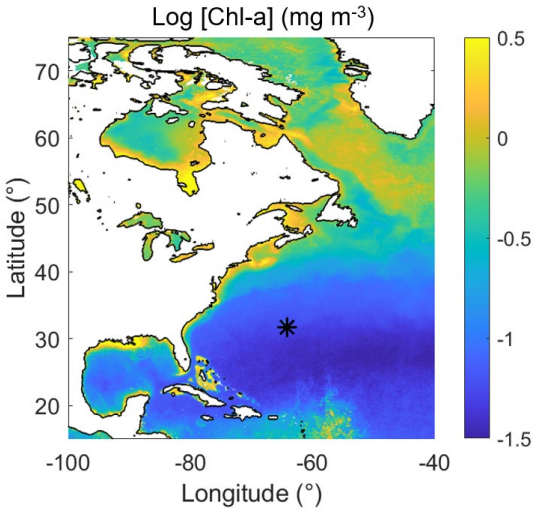

Figure S1. Climatological chlorophyll-*a* concentrations in the northern Atlantic Ocean for average July conditions. The BATS site is marked with *. Data from Melin (46), available at: http://data.europa.eu/89h/d6f9abd9-777c-4a0c-a5f7-669612f83307

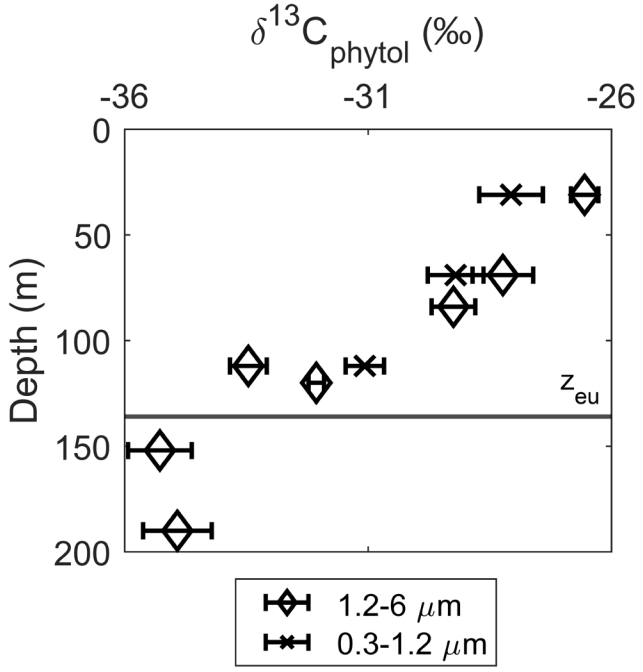

Figure S2. $\delta^{13}C$ values of phytol from 0.3-1.2 µm and 1.2-6 µm size fractions. Error bars represent 1σ. Horizontal line represents the 0.1% light level and base of the euphotic zone.

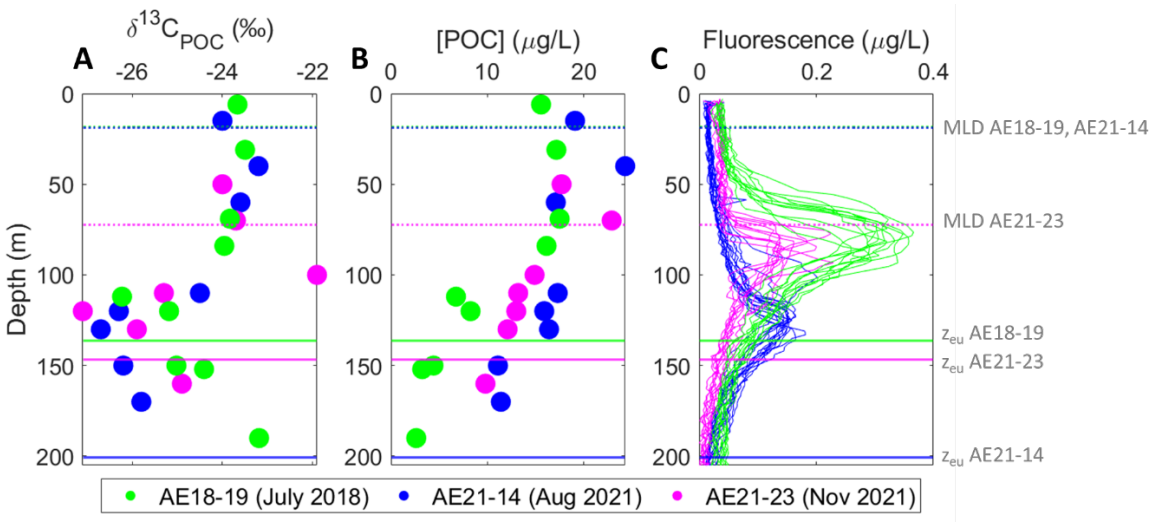

Figure S3. Comparison of $\delta^{13}C_{POC}$ values, POC concentrations, and CTD chlorophyll fluorescence data from AE18-19, AE21-14, and AE21-23. Solid lines represent euphotic depths (z_{eu}) and dotted lines are mixed layer depths (MLD) for each cruise. AE18-19 data are from 1.2-6 µm POM collected by in-situ pumps, while AE21-14 and AE21-23 data are from total POM collected from Niskin bottles on the rosette.

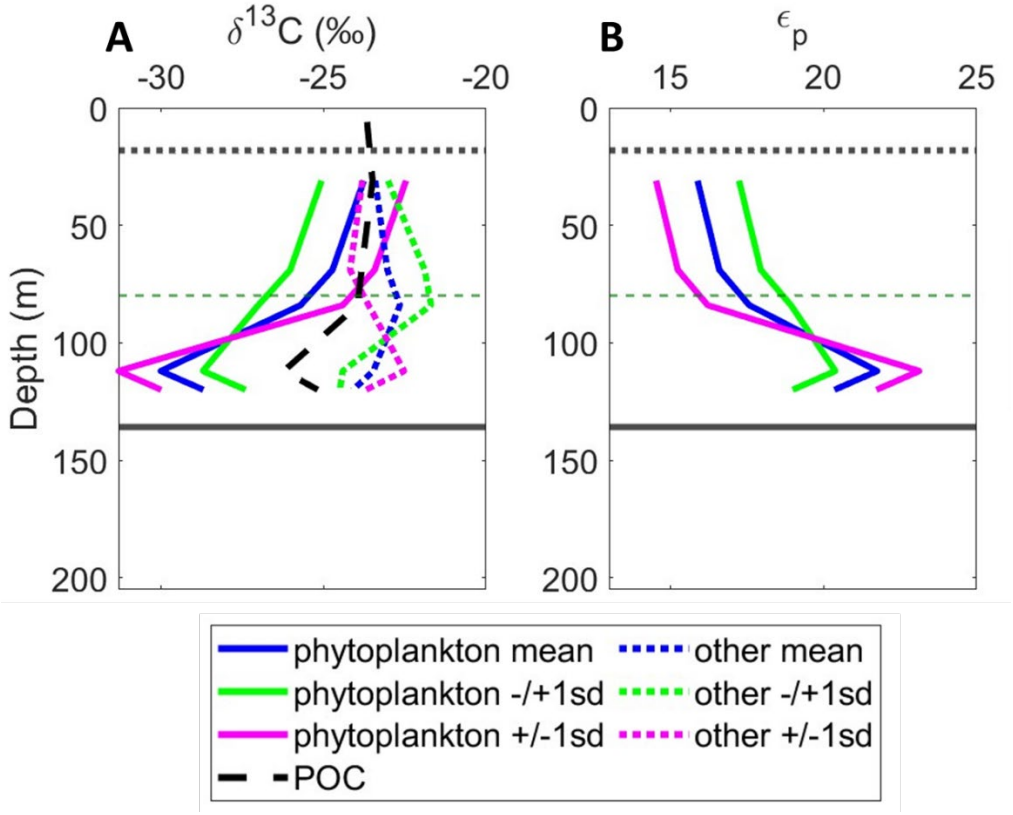

Figure S4. Consequences of assuming constant vs. varying offset between $\delta^{13}C$ values of phytol and phytoplankton biomass ($\Delta\delta^{13}C_{p\text{-}phytol}$; Equation 1, main text): effects on calculated $\delta^{13}C$ values of phytoplankton and non-phytoplankton organic matter ("other"; A), and ε_p (B). Calculations are described in SI 2.1 and SI 2.5. **(A)** Calculated $\delta^{13}C$ values of 1.2-6 µm phytoplankton biomass (solid lines) and other, non-phytoplankton POC (dotted lines) with a $\Delta\delta^{13}C_{p\text{-}phytol}$ value of, in blue: 3.5‰ throughout the euphotic zone [mean from Witkowski et al. **(7)**] and two extreme cases of varying $\Delta\delta^{13}C_{p\text{-}phytol}$, in green: 0.9‰ at 0-90 m (mean -1σ) and 6.1‰ at 90-120 m (mean +1σ); in magenta: 6.1‰ (mean +1σ) at 0-90 m and 0.9‰ (mean -1σ) at 90-120 m. Measured total 1.2-6 µm POC is plotted in the black dashed line. **(B)** ε_p calculated from phytoplankton biomass based on the variable $\Delta\delta^{13}C_{p\text{-}phytol}$ used in panel A.

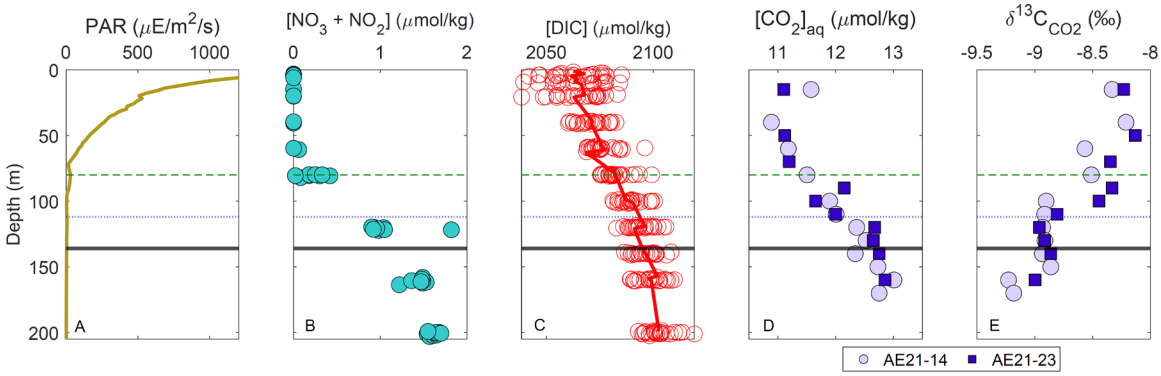

Figure S5. Profiles of environmental parameters over depth at the Bermuda Atlantic Time-series Study (BATS) site. Photosynthetically active radiation (PAR) and nitrate data are from AE18-19 (July 2018), CO_2 concentration and $\delta^{13}C$ values are from AE21-14 and AE21-23, and DIC concentration data are from the BATS bottle file from June/July 2012-2019. $[CO_2]$ was calculated via CO2SYS **(36)** from measured DIC and alkalinity concentrations, and $\delta^{13}C_{CO2}$ values were calculated from $\delta^{13}C_{DIC}$ values and temperature **(16, 40, 41)**. Dashed green line denotes the depth of the deep chlorophyll maximum, blue dotted line denotes the depth of the carbon isotope minimum in POC, and the solid black line denotes the euphotic depth (z_{eu}).

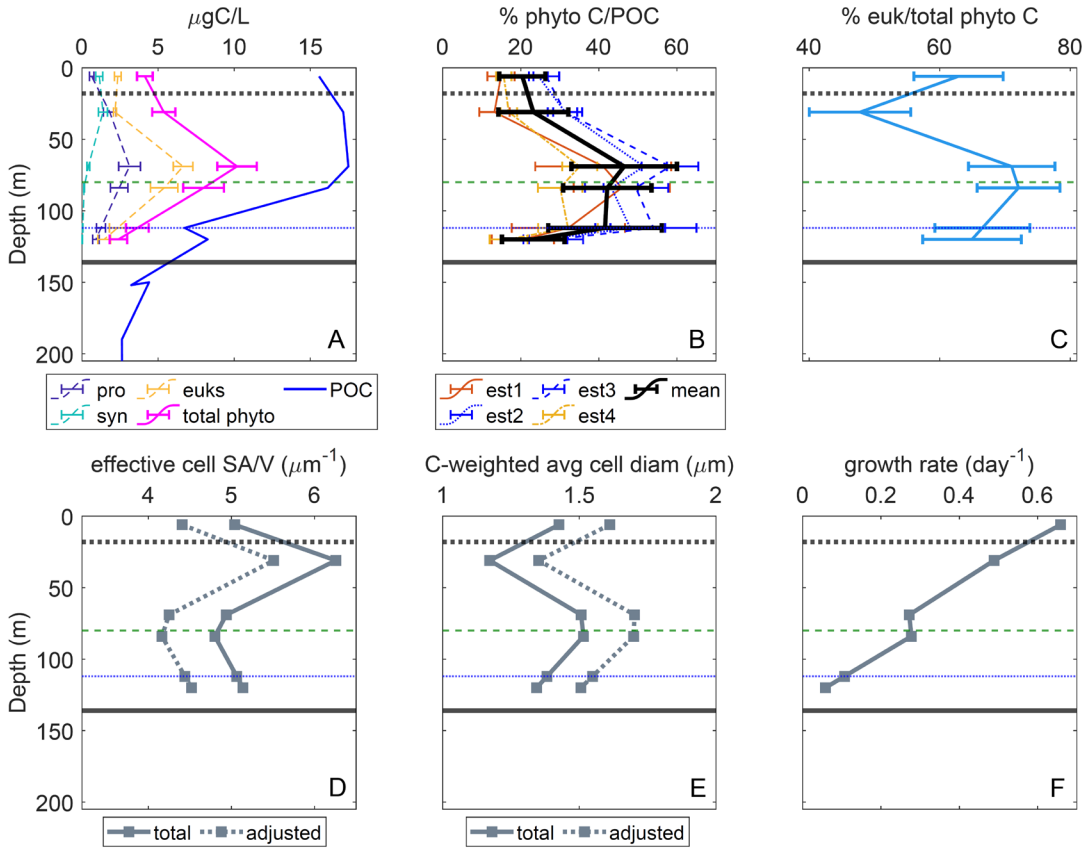

Figure S6. Variations in phytoplankton biomass carbon, cell size, and growth rates over depth in the euphotic zone at the BATS site, July 2018. Horizontal lines on all plots are as follows: grey dotted is the depth of the mixed layer, dashed green is the depth of the deep chlorophyll maximum, blue dotted is the depth of the minimum carbon isotope value in both bulk POC and phytol, and solid grey is the depth of the euphotic zone. **Calculations for all panels are described in more detail SI 2.3. (A)** Estimates of *Prochlorococcus* (Pro), *Synechococcus* (Syn), total eukaryotic phytoplankton (euks), and summed phytoplankton biomass captured in 1.2-6 μm particles, as calculated from flow cytometry cell abundances and previously published average cell diameters **(10)**. Total POC concentrations were measured in 1.2-6 μm particles. **(B)** Percent of total POC in the 1.2-6 μm size fraction comprised of phytoplankton biomass. Estimate 1 (est1) is based on CTD chlorophyll fluorescence and chl:C ratios **(9, 47)**. Estimates 2-3 are based on flow cytometry cell abundances, previously published average cell diameters **(10)**, and biovolume to biomass conversions in Verity et al. **(11)**, with estimate 3 adjusted for only the 1.2-6 μm size fraction (SI 2.3). Estimate 4 is based on flow cytometry cell abundances, previously published average cell diameters **(10)**, and biovolume to biomass conversions in Worden et al. **(13)**, adjusted for only the 1.2-6 μm size fraction (SI 2.3). **(C)** Percentage of total 1.2-6 μm phytoplankton carbon comprised of eukaryotic phytoplankton biomass, calculated as the average of estimates 3 and 4 in panel B (see section SI 2.3 for details). **(D)** Estimates of average effective surface area to volume ratio of phytoplankton cells; total refers to all phytoplankton while adjusted refers to phytoplankton in the 1.2-6 μm size fraction. **(E)** Biomass-weighted average phytoplankton cell diameter; total refers to all phytoplankton while adjusted refers to estimated phytoplankton in the 1.2-6 μm size fraction (see section SI 2.3 for details). **(F)** Phytoplankton growth rate calculated from measured net primary production (BATS bottle file June/July 2018-2019 average) and estimates of phytoplankton biomass.

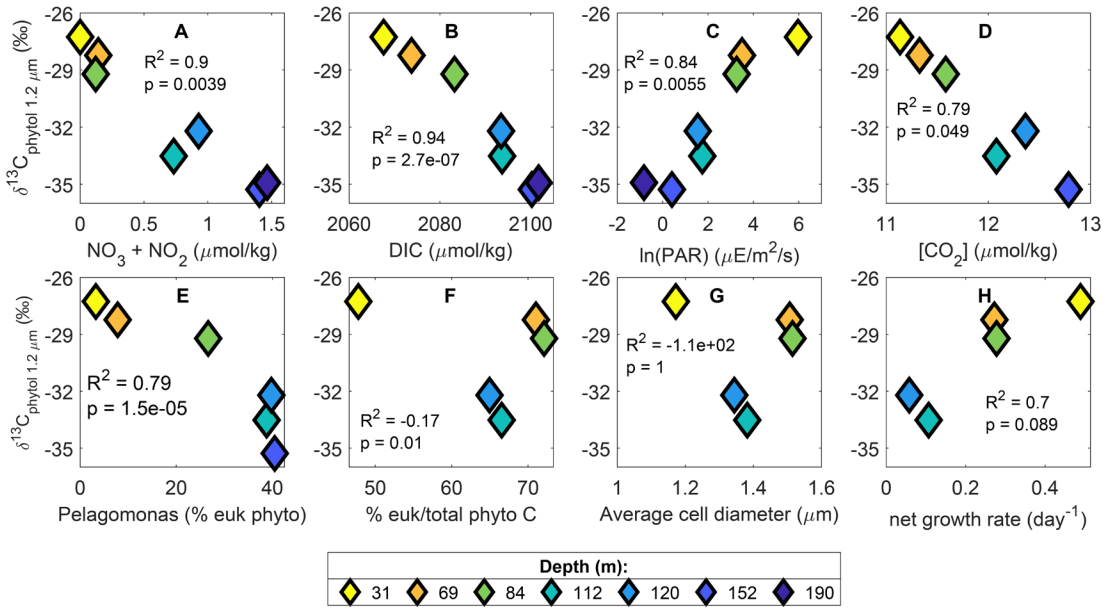

Figure S7. Relationships between $\delta^{13}C_{phytol}$ values of 1.2-6 µm particles and environmental parameters or phytoplankton community composition. Colors of symbols indicate depth of collection. R^2 and p values are based on orthogonal regression fit to data using MATLAB function linortfit2 (48). Panels D-E have no data at 190 m due to data availability. Panels F-H have no data at 152 or 190 m because the deepest depth of enumeration for cell abundances was 120 m. **A-D:** NO_3^-+NO_2^- concentration and photosynthetically available radiation (PAR) are from cruise AE18-19 (July 2018). CO_2 concentration is calculated from measured DIC concentrations from AE21-14 (August 2021). Dissolved inorganic carbon (DIC) concentration is averaged from BATS cruises June/July 2012-2019. **E:** *Pelagomonas* relative abundance was calculated from size-fractionated v4 ASVs as a percentage of all plastid ASVs. **F:** Percentage of total phytoplankton carbon that is comprised of eukaryotic phytoplankton was estimated via measured cell abundances (see SI 2.3). **G:** Phytoplankton growth rate was calculated from measured net primary production (BATS cruises June/July 2018-2019 average) and phytoplankton biomass estimates (see SI 2.3).

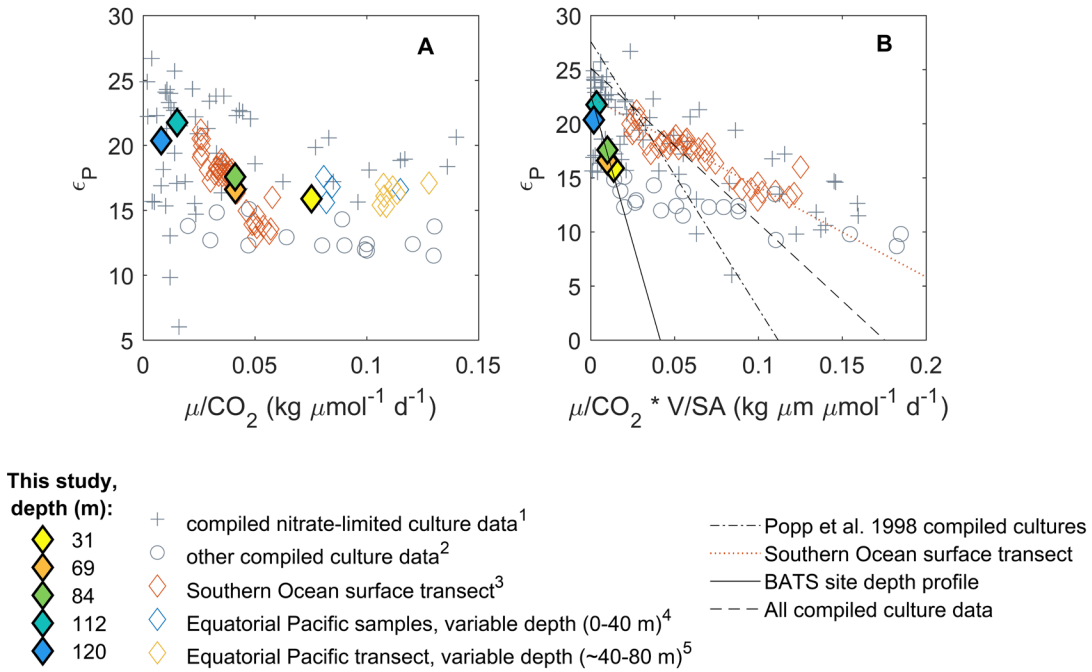

Figure S8. Relationships plotted in main text Figure 4, with the addition of light-limited culture data. Relationships between photosynthetic carbon isotope fractionation (ε_p) and (A) growth rate (μ) divided by CO_2 concentration, and (B) growth rate divided by CO_2 concentration, divided by the phytoplankton surface area (SA) to volume (V) ratio. For our data, specific growth rates were calculated via measured net primary production and estimated phytoplankton biomass from measured cell abundances (SI 2.3). Surface area to volume ratios were also estimated via cell abundances (SI 2.3)**.** Phytoplankton culture data is compiled from nitrate-limited, continuous light chemostat cultures; nutrient-replete dilute batch cultures with light:dark cycles under saturating light; and nutrient-replete, light-limited dilute batch cultures. Environmental data is from this study (both panels, filled diamonds); surface samples in the Southern Ocean (both panels), and, for panel A only due to lack of cell size data, various depths in the equatorial Pacific. Mathematical relationships modeled after Popp et al. **(49)**, though linear relationships here are fit using orthogonal linear regression [MATLAB function linortfit2; **(48)**], which results in a slope and intercept for compiled culture data different than that in Popp et al. **(49)**. Superscripts in legend denote data from: **[1]** Bidigare et al. **(50)**; Laws et al. **(15)**; Popp et al. **(49)**; Wilkes et al. **(51)**; Hurley et al. **(52)**; **[2]** Burkhardt et al. **(53)**; Riebesell et al. **(54, 55)**; **[3]** Popp et al. **(18)**; **[4]** Bidigare et al. **(17)**; **[5]** Laws et al. **(14)**.

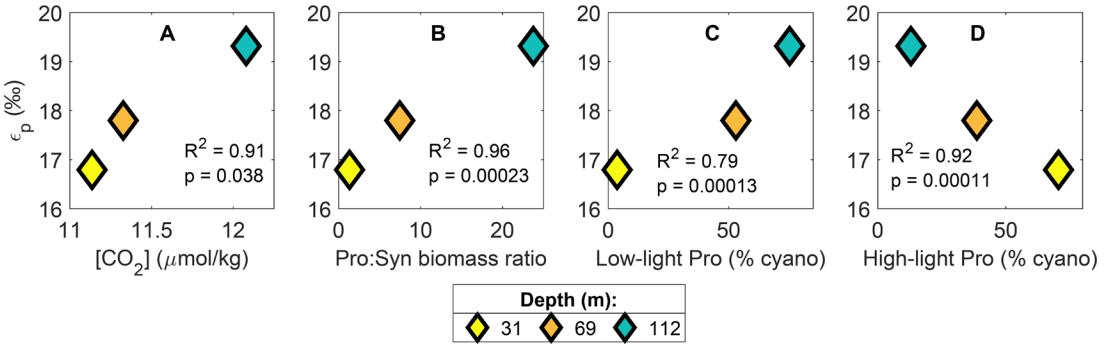

Figure S9. Relationships between ε_p values of 0.3-1.2 µm particles and environmental parameters or cyanobacterial community composition. Color of symbols indicates depth of collection. R^2 and p values are based on orthogonal regression fit to data using MATLAB function linortfit2 **(48)**. **A:** CO_2 concentration was calculated from measured DIC concentrations from AE21-14 (August 2021) via CO2SYS [**(36)**; SI 4.3]. **B:** Ratio of Pro:Syn biomass as calculated via phytoplankton biomass estimates from cell abundances and average cell diameters for the subset for which all measurements were available (explained in SI 2.3). **C:** Relative abundance of low-light *Prochlorococcus* ecotypes calculated from whole seawater v1v2 16S rRNA ASVs as a percent of all cyanobacteria ASVs. **D:** Relative abundance of high-light *Prochlorococcus* ecotypes calculated from whole seawater v1v2 ASVs as a percentage of all cyanobacteria ASVs.

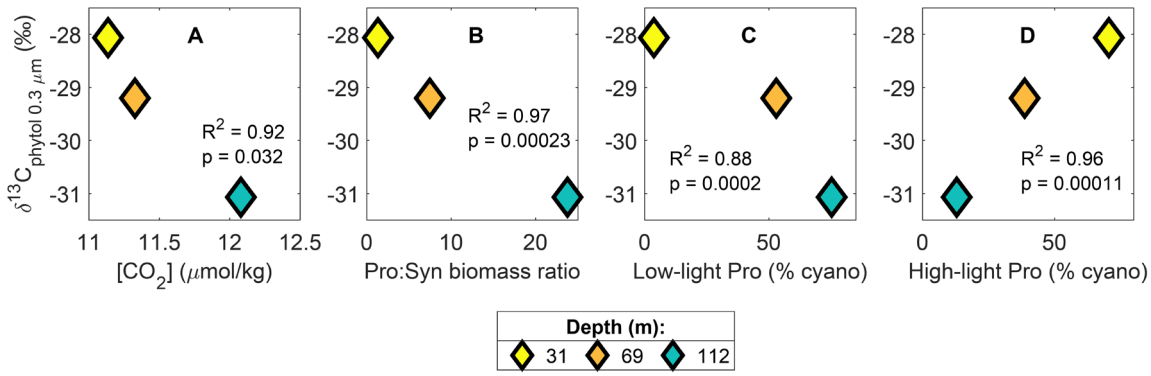

Figure S10. Relationships between $\delta^{13}C_{phytol}$ values of 0.3-1.2 µm particles and environmental parameters or cyanobacterial community composition. Color of symbols indicates depth of collection. R^2 and p values are based on orthogonal regression fit to data using MATLAB function linortfit2 **(48)**. **A:** CO_2 concentration was calculated from measured DIC concentrations from AE21-14 (August 2021) via CO2SYS [**(36)**; SI 4.3]. **B:** Ratio of Pro:Syn biomass as calculated via phytoplankton biomass estimates from cell abundances and average cell diameters for the subset for which all measurements were available (explained in SI 2.3). **C:** Relative abundance of low-light *Prochlorococcus* ecotypes calculated from whole seawater v1v2 16S rRNA ASVs as a percent of all cyanobacteria ASVs. **D:** Relative abundance of high-light *Prochlorococcus* ecotypes calculated from whole seawater v1v2 ASVs as a percentage of all cyanobacteria ASVs.

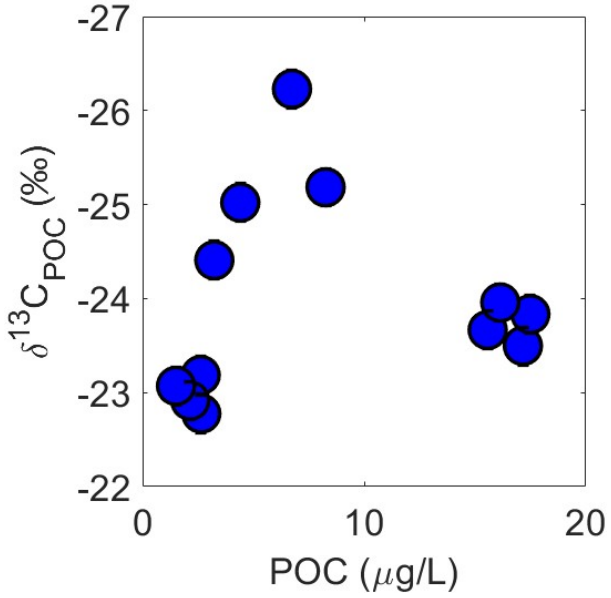

Figure S11. Measured $\delta^{13}C_{POC}$ values vs POC concentrations in 1.2-6 μm particles.

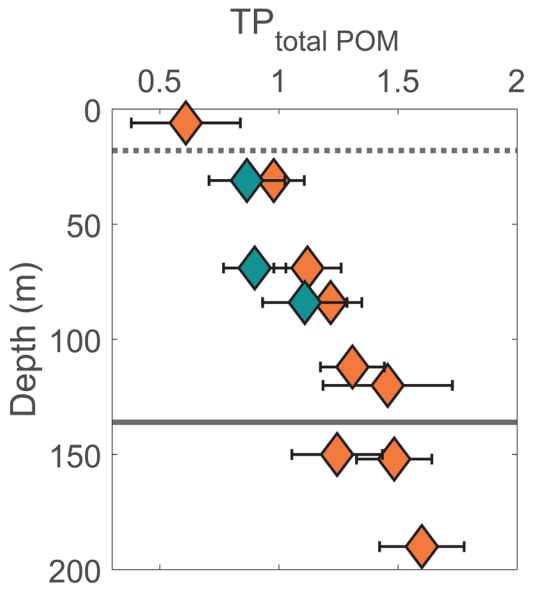

Figure S12. Trophic position (TP) of measured total POM as calculated from $\delta^{15}N$ values of individual AAs (Equation 4, Materials and Methods). Orange denotes 1.2-6 μm particles and teal denotes 0.3-1.2 μm particles.

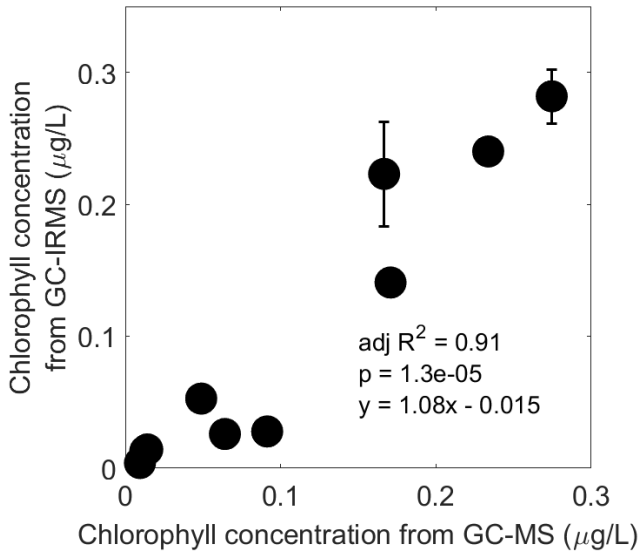

Figure S13. Calculated chlorophyll concentrations from measured phytol concentrations from GC-IRMS analysis vs those from GC-MS analysis, includes 0.3-1.2 and 1.2-6 µm data. Error bars represent 1σ of replicate analyses.

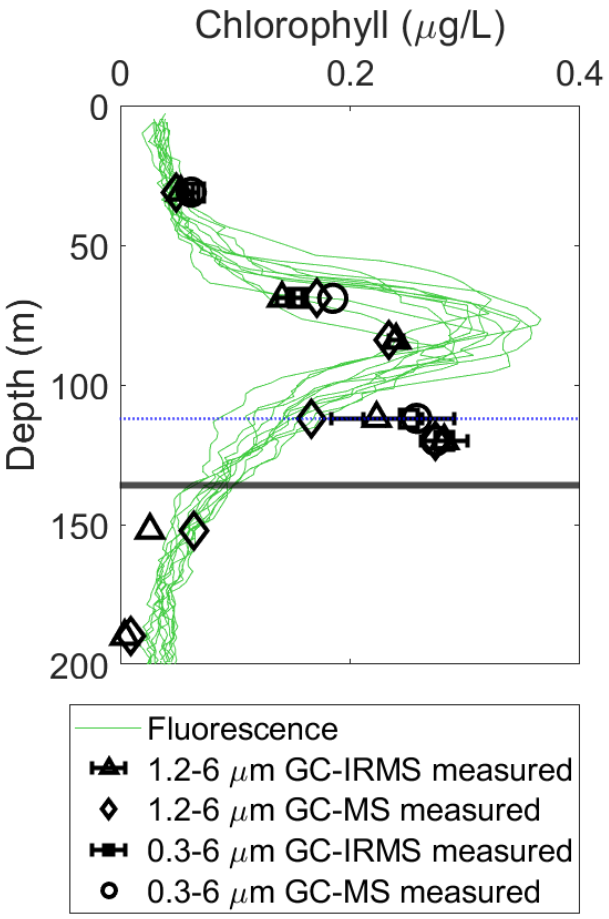

Figure S14. Calculated chlorophyll concentrations from measured phytol concentrations (analyzed two ways: GC-MS and GC-IRMS) in the 1.2-6 μm size fraction plotted over CTD fluorescence from all casts on the cruise. Solid black line marks the euphotic depth. Dotted blue line marks depth of the isotope minimum.

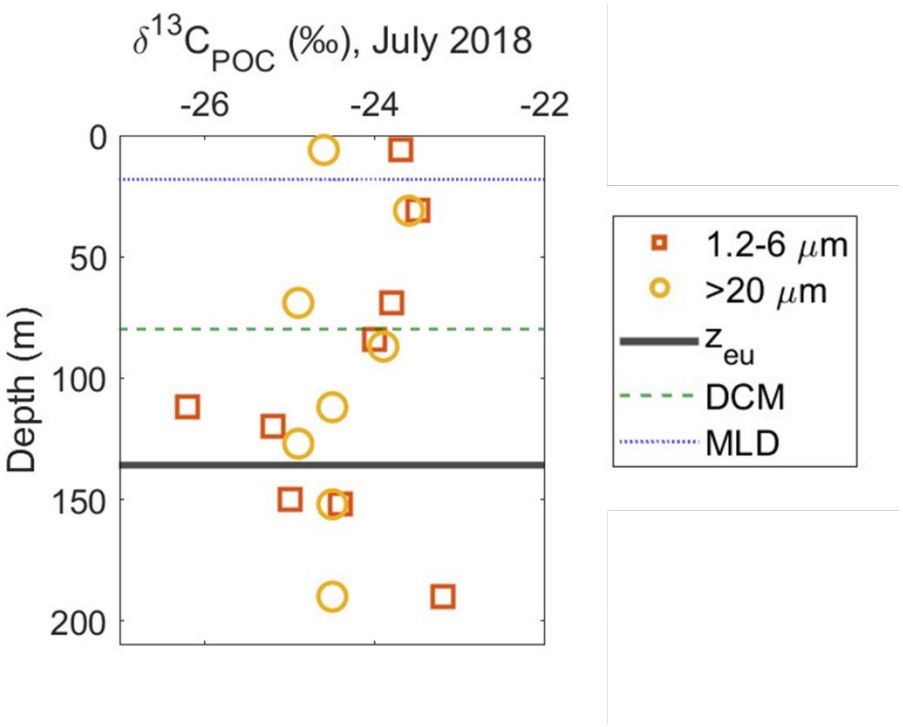

Figure S15. $\delta^{13}C_{POC}$ values of 1.2-6 and >20 µm particles within the upper 200 m during July 2018.

Sample info					Measured phytol concentration (ng/L) FROM GC-MS						Measured phytol concentration (ng/L) FROM GC-IRMS						standard deviation (ng/L) FROM GC-IRMS					
Close Lab Sample ID	**Split type**	**Size fraction**	**Depth (m)**	**Depth uncertainty (m)**	**F7 unsap**	**F7 sap**	**F8 unsap**	**F8 sap**	**F9-10 unsap**	**F9-10 sap**	**F7 unsap**	**F7 sap**	**F8 unsap**	**F8 sap**	**F9-10 unsap**	**F9-10 sap**	**F7 unsap**	**F7 sap**	**F8 unsap**	**F8 sap**	**F9-10 unsap**	**F9-10 sap**
19-02	frozen	1.2	31	2	BLD	0.9	BLD	5.0	BLD	10.2	n/a	BLQ	n/a	3.9	n/a	12.6	n/a	n/a	n/a	n/a	n/a	0.7
19-01	frozen	1.2	69	2	BLD	4.9	BLD	BLD	BLD	40.2	n/a	n/a	n/a	11.6	n/a	30.2	n/a	n/a	n/a	n/a	n/a	1.3
19-09	frozen	1.2	84	8	BLQ	BLD	BLD	12.4	BLQ	65.1	n/a	n/a	n/a	5.5	n/a	74.2	n/a	n/a	n/a	n/a	n/a	2.0
19-06	frozen	1.2	112	2	BLD	BLD	BLD	8.4	2.0	46.9	n/a	n/a	n/a	2.7	n/a	71.3	n/a	n/a	n/a	n/a	n/a	13.1
19-08	frozen	1.2	120	8	BLQ	2.9	BLQ	21.7	BLQ	66.5	n/a	n/a	n/a	34.3	n/a	56.3	n/a	n/a	n/a	n/a	n/a	6.8
19-05	frozen	1.2	152	2	n/a	0.6	n/a	2.5	n/a	18.1	n/a	BLQ	n/a	n/a	n/a	5.4	n/a	n/a	n/a	n/a	n/a	n/a
19-04	frozen	1.2	190	2	BLD	BLD	BLD	BLD	BLQ	3.1	n/a	n/a	n/a	BLD	n/a	1.3	n/a	n/a	n/a	n/a	n/a	n/a
19-11	frozen	1.2	BLANK	n/a	BLD	BLD	BLD	BLD	BLD	BLD	n/a	n/a	n/a	n/a	n/a	n/a	n/a	n/a	n/a	n/a	n/a	n/a
19-30	freeze-dried	0.3	31	2	n/a	1.4	n/a	0.9	n/a	n/a	n/a	n/a	n/a	n/a	n/a	1.9	n/a	n/a	n/a	n/a	n/a	n/a
19-29	freeze-dried	0.3	69	2	n/a	0.8	n/a	1.3	n/a	n/a	n/a	n/a	n/a	n/a	n/a	2.7	n/a	n/a	n/a	n/a	n/a	n/a
19-34	freeze-dried	0.3	112	2	n/a	0.4	n/a	1.4	n/a	28.5	n/a	n/a	n/a	n/a	n/a	7.4	n/a	n/a	n/a	n/a	n/a	0.8
19-34	frozen	0.3	112	2	n/a	n/a	n/a	n/a	n/a	n/a	n/a	n/a	n/a	n/a	n/a	n/a	n/a	n/a	n/a	n/a	n/a	n/a

Table S1. measured phytol concentrations in all samples from GC-MS and GC-IRMS; polarity fractions are denoted by F7 (alcohol fraction), F8 (sterol fraction) and F9-10 (intact polar lipid fraction). “Sap” and “unsap” denote “saponified” and “unsaponified”, respectively. BLQ indicates the sample concentration was below the limit of quantitation and BLD indicates the sample concentration was below the limit of detection. n/a indicates the sample was not analyzed. Free phytol would be expected in F7, saponified and unsaponified, while phytol from intact chlorophyll would be expected in F9-10, saponified only; reported $\delta^{13}C_{phytol}$ data are the weighted average of measured $\delta^{13}C_{phytol}$ values in F9-10 and F8 saponified fractions, where phytol was present.

Correlations with 1.2-6 µm d13Cphytol						
Variable	**R2**	**Adj R2**	**pval**	**slope**	**intercept**	**n**
NO3	0.92	0.90	3.90E-03	-5.5	-27.7	7
DIC	0.95	0.94	2.69E-07	-0.2	475.45	7
PAR	0.87	0.84	5.52E-03	1.5	-34.9	7
CO2	0.84	0.81	0.05	-5.6	34.9	6
Pelagomonas v4 rel ab	0.84	0.79	1.5E-05	-0.2	-26.39	6
percent euk/total phyto C	0.12	-0.17	0.01	-0.1	-23.6	5
average cell size	-81.10	-108.46	1.00	-173.3	209.7	5
net growth rates	0.78	0.70	0.09	17.4	-34.3	5

Table S2. R^2, p-values, slopes, and intercepts for linear models fit to $\delta^{13}C_{phytol}$ values vs other variables for 1.2-6 µm samples using MATLAB function linortfit2 **(48)**.

Correlations with 1.2-6 µm Ep						
Variable	**R2**	**Adj R2**	**pval**	**slope**	**intercept**	**n**
NO3	0.90	0.88	0.01	5.8	16.2	6
DIC	0.92	0.90	6.97E-06	0.2	-468.5	6
PAR	0.84	0.79	0.02	-1.6	23.9	6
CO2	0.91	0.89	0.01	5.0	-40.4	6
Pelagomonas v4 rel ab	0.81	0.77	1.71E-05	0.2	15.1	6
percent euk/total phyto C	0.11	-0.18	0.01	0.1	12.6	5
average cell size	-92.58	-123.77	1.00	174.4	-222.7	5
net growth rates	0.74	0.66	0.11	-16.6	22.6	5

Table S3. R^2, p-values, slopes, and intercepts for linear models fit to ε_p values vs other variables for 1.2-6 µm samples using MATLAB function linortfit2 (48).

Correlations with 0.3-1.2 µm d13Cphytol						
Variable	**R2**	**Adj R2**	**pval**	**slope**	**intercept**	**n**
CO2	0.96	0.92	0.03	-3.1	6.10	3
Pro:Syn ratio	0.99	0.97	2.29E-04	-0.1	-28.04	3
Low-light Pro ecotypes	0.88	0.76	2.05E-04	0.0	-27.736	3
High-light Pro ecotypes	0.96	0.92	1.09E-04	0.1	-31.541	3

Table S4. R^2, p-values, slopes, and intercepts for linear models fit to $\delta^{13}C_{phytol}$ values vs other variables for 0.3-1.2 µm samples using MATLAB function linortfit2 **(48)**.

Correlations with 0.3-1.2 µm Ep						
Variable	**R2**	**Adj R2**	**pval**	**slope**	**intercept**	**n**
CO2	0.95	0.91	0.04	2.6	-11.88	3
Pro:Syn ratio	0.98	0.96	2.30E-04	0.1	16.79	3
Low-light Pro ecotypes	0.89	0.79	1.27E-04	0.0	16.525	3
High-light Pro ecotypes	0.96	0.92	1.09E-04	0.1	-31.541	3

Table S5. R^2, p-values, slopes, and intercepts for linear models fit to ε_p values vs other variables for 0.3-1.2 µm samples using MATLAB function linortfit2 **(48)**.

Correlations between εp and μ/[CO2] * (SA/V) 1						
data	R2	Adj R2	p-value	slope	intercept	n
BATS depth profile, 1.2-6 μm particles	0.85	0.80	0.05	-546.44	22.6	5
Southern Ocean surface transect, >1 μm particles	0.77	0.76	1.87E-05	-82.97	22.4	36
All compiled culture data (eukaryotes)	0.47	0.46	0.01	-124.81	25.2	54
Popp et al. 1998 culture data (eukaryotes)	0.60	0.58	0.02	-246.90	27.6	24
BATS depth profile with 17% surface area available, 1.2-6 μm particles	0.85	0.80	0.05	-92.89	22.6	5

Table S6. R^2, p-values, slopes, and intercepts for linear models fit to ε_p values vs $\mu/[CO_2] * (SA/V)^{-1}$ for 1.2-6 μm samples using MATLAB function linortfit2 **(48)**. "All compiled culture data" refers to all compiled data presented in the main text.

SI References

1. I. Tolosa, *et al.*, Distribution of lipid biomarkers and carbon isotope fractionation in contrasting trophic environments of the South East Pacific. *Biogeosciences* **5**, 949–968 (2008).

2. W. Hägele, D. Schmid, F. Drissler, J. Nauš, H. C. Wolf, Optical Spectra of Chlorophyll a and b Molecules and Complexes in PMMA and MTHF. *Zeitschrift für Naturforschung A* **33**, 1197–1205 (1978).

3. R. R. Bidigare, M. C. Kennicutt, W. L. Keeney-Kennicutt, S. A. Macko, Isolation and purification of chlorophylls a and b for the determination of stable carbon and nitrogen isotope compositions. *Anal. Chem.* **63**, 130–133 (1991).

4. C. S. Yentsch, Distribution of chlorophyll and phaeophytin in the open ocean. *Deep Sea Research and Oceanographic Abstracts* **12**, 653–666 (1965).

5. M. Vernet, C. J. Lorenzen, The relative abundance of pheophorbide a and pheophytin a in temperate marine waters1. *Limnology and Oceanography* **32**, 352–358 (1987).

6. J. R. Sargent, S. Falk-Petersen, Ecological investigations on the zooplankton community in balsfjorden, northern Norway: Lipids and fatty acids in Meganyctiphanes norvegica, Thysanoessa raschi and T. inermis during mid-winter. *Mar. Biol.* **62**, 131–137 (1981).

7. C. R. Witkowski, J. W. H. Weijers, B. Blais, S. Schouten, J. S. Sinninghe Damsté, Molecular fossils from phytoplankton reveal secular P_{CO_2} trend over the Phanerozoic. *Sci. Adv.* **4**, eaat4556 (2018).

8. T. C. Malone, S. E. Pike, D. J. Conley, Transient variations in phytoplankton productivity at the JGOFS Bermuda time series station. *Deep Sea Research Part I: Oceanographic Research Papers* **40**, 903–924 (1993).

9. K. Gundersen, K. M. Orcutt, D. A. Purdie, A. F. Michaels, A. H. Knap, Particulate organic carbon mass distribution at the Bermuda Atlantic Time-series Study (BATS) site. *Deep Sea Research Part II: Topical Studies in Oceanography* **48**, 1697–1718 (2001).

10. M. D. DuRand, R. J. Olson, S. W. Chisholm, Phytoplankton population dynamics at the Bermuda Atlantic Time-series station in the Sargasso Sea. *Deep Sea Research Part II: Topical Studies in Oceanography* **48**, 1983–2003 (2001).

11. P. G. Verity, *et al.*, Relationships between cell volume and the carbon and nitrogen content of marine photosynthetic nanoplankton. *Limnology and Oceanography* **37**, 1434–1446 (1992).

12. R. W. Sheldon, Size Separation of Marine Seston by Membrane and Glass-Fiber Filters1. *Limnology and Oceanography* **17**, 494–498 (1972).

13. A. Z. Worden, J. K. Nolan, B. Palenik, Assessing the dynamics and ecology of marine picophytoplankton: The importance of the eukaryotic component. *Limnology and Oceanography* **49**, 168–179 (2004).

14. E. A. Laws, B. N. Popp, J. R. R. Bidigare, M. C. Kennicutt, S. A. Macko, Dependence of phytoplankton carbon isotopic composition on growth rate and $[CO_2]$aq : Theoretical

considerations and experimental results. *Geochimica et Cosmochimica Acta* **59**, 1131–1138 (1995).

15. E. A. Laws, R. R. Bidigare, B. N. Popp, Effect of growth rate and CO_2 concentration on carbon isotopic fractionation by the marine diatom *Phaeodactylum tricornutum*. *Limnol. Oceanogr.* **42**, 1552–1560 (1997).

16. G. H. Rau, U. Riebesell, D. Wolf-Gladrow, A model of photosynthetic 13C fractionation by marine phytoplankton based on diffusive molecular CO2 uptake. *Mar. Ecol. Prog. Ser.* **133**, 275–285 (1996).

17. R. R. Bidigare, *et al.*, Iron-stimulated changes in 13C fractionation and export by equatorial Pacific phytoplankton: Toward a paleogrowth rate proxy. **14**, 589–595 (1999).

18. B. N. Popp, *et al.*, Controls on the carbon isotopic composition of southern ocean phytoplankton. *Global Biogeochemical Cycles* **13**, 827–843 (1999).

19. S. J. Giovannoni, M. S. Rappe, K. L. Vergin, N. L. Adair, 16S rRNA genes reveal stratified open ocean bacterioplankton populations related to the Green Non-Sulfur bacteria. *Proceedings of the National Academy of Sciences of the United States of America* **93**, 7979–7984 (1996).

20. A. Apprill, S. McNally, R. Parsons, L. Weber, Minor revision to V4 region SSU rRNA 806R gene primer greatly increases detection of SAR11 bacterioplankton. *Aquat. Microb. Ecol.* **75**, 129–137 (2015).

21. A. E. Parada, D. M. Needham, J. A. Fuhrman, Every base matters: assessing small subunit rRNA primers for marine microbiomes with mock communities, time series and global field samples: Primers for marine microbiome studies. *Environ Microbiol* **18**, 1403–1414 (2016).

22. E. K. Wear, E. G. Wilbanks, C. E. Nelson, C. A. Carlson, Primer selection impacts specific population abundances but not community dynamics in a monthly time-series 16S rRNA gene amplicon analysis of coastal marine bacterioplankton. *Environmental Microbiology* **20**, 2709–2726 (2018).

23. J. McNichol, P. M. Berube, S. J. Biller, J. A. Fuhrman, Evaluating and Improving Small Subunit rRNA PCR Primer Coverage for Bacteria, Archaea, and Eukaryotes Using Metagenomes from Global Ocean Surveys. *mSystems* **6**, e00565-21 (2021).

24. B. J. Callahan, *et al.*, DADA2: High-resolution sample inference from Illumina amplicon data. *Nat Methods* **13**, 581–583 (2016).

25. C. Quast, *et al.*, The SILVA ribosomal RNA gene database project: improved data processing and web-based tools. *Nucleic Acids Research* **41**, D590–D596 (2012).

26. K. L. Vergin, *et al.*, High-resolution SAR11 ecotype dynamics at the Bermuda Atlantic Time-series Study site by phylogenetic placement of pyrosequences. *ISME J* **7**, 1322–1332 (2013).

27. L. M. Bolaños, *et al.*, Seasonality of the Microbial Community Composition in the North Atlantic. *Front. Mar. Sci.* **8**, 624164 (2021).

28. Z. Landry, B. K. Swan, G. J. Herndl, R. Stepanauskas, S. J. Giovannoni, SAR202 Genomes from the Dark Ocean Predict Pathways for the Oxidation of Recalcitrant Dissolved Organic Matter. *mBio* **8**, e00413-17 (2017).

29. S. Sudek, *et al.*, Cyanobacterial distributions along a physico-chemical gradient in the Northeastern Pacific Ocean: Cyanobacterial distributions in the Pacific Ocean. *Environ Microbiol* **17**, 3692–3707 (2015).

30. L. Guillou, *et al.*, The Protist Ribosomal Reference database (PR2): a catalog of unicellular eukaryote Small Sub-Unit rRNA sequences with curated taxonomy. *Nucleic Acids Research* **41**, D597–D604 (2012).

31. H. Daims, A. Brühl, R. Amann, K.-H. Schleifer, M. Wagner, The Domain-specific Probe EUB338 is Insufficient for the Detection of all Bacteria: Development and Evaluation of a more Comprehensive Probe Set. *Systematic and Applied Microbiology* **22**, 434–444 (1999).

32. F. A. Matsen, R. B. Kodner, E. V. Armbrust, pplacer: linear time maximum-likelihood and Bayesian phylogenetic placement of sequences onto a fixed reference tree. *BMC Bioinformatics* **11**, 538 (2010).

33. C. J. Choi, *et al.*, Seasonal and Geographical Transitions in Eukaryotic Phytoplankton Community Structure in the Atlantic and Pacific Oceans. *Front. Microbiol.* **11**, 542372 (2020).

34. , "BATS Method Manual (Version 4)" (US Joint Global Ocean Flux Study & Bermuda Atlantic Time-series Study, 1997).

35. M. I. Scranton, *et al.*, Anomalous δ13C in Particulate Organic Carbon at the Chemoautotrophy Maximum in the Cariaco Basin. *Journal of Geophysical Research: Biogeosciences* **125**, e2019JG005276 (2020).

36. S. Van Heuven, D. Pierrot, J. W. B. Rae, E. Lewis, D. W. R. Wallace, MATLAB Program Developed for CO2 System Calculations. ORNL/CDIAC-105b. (2011) https:/doi.org/10.3334/CDIAC/OTG.CO2SYS_MATLAB_V1.1 (June 14, 2022).

37. W.-J. Cai, Y. Wang, The chemistry, fluxes, and sources of carbon dioxide in the estuarine waters of the Satilla and Altamaha Rivers, Georgia. *Limnol. Oceanogr.* **43**, 657–668 (1998).

38. A. G. Dickson, Thermodynamics of the dissociation of boric acid in synthetic seawater from 273.15 to 318.15 K. *Deep Sea Research Part A. Oceanographic Research Papers* **37**, 755–766 (1990).

39. L. R. Uppström, The boron/chlorinity ratio of deep-sea water from the Pacific Ocean. *Deep Sea Research and Oceanographic Abstracts* **21**, 161–162 (1974).

40. W. G. Mook, J. C. Bommerson, W. H. Staverman, Carbon isotope fractionation between dissolved bicarbonate and gaseous carbon dioxide. *Earth and Planetary Science Letters* **22**, 169–176 (1974).

41. T. O'Leary, T. W. Trull, F. B. Griffiths, B. Tilbrook, A. T. Revill, Euphotic zone variations in bulk and compound-specific δ13C of suspended organic matter in the subantarctic ocean, south of Australia. *Journal of Geophysical Research* **106**, 31669–31684 (2001).

42. C. C. S. Hannides, B. N. Popp, C. A. Choy, J. C. Drazen, Midwater zooplankton and suspended particle dynamics in the North Pacific Subtropical Gyre: A stable isotope perspective. *Limnol. Oceanogr.* **58**, 1931–1946 (2013).

43. S. C. Doherty, A. E. Maas, D. K. Steinberg, B. N. Popp, H. G. Close, Distinguishing zooplankton fecal pellets as a component of the biological pump using compound-specific isotope analysis of amino acids. *Limnology and Oceanography* **66**, 2827–2841 (2021).

44. P. K. Wojtal, *et al.*, Deconvolving mechanisms of particle flux attenuation using nitrogen isotope analyses of amino acids. *Limnology & Oceanography* **68**, 1965–1981 (2023).

45. B. N. Popp, *et al.*, "Insight into the Trophic Ecology of Yellowfin Tuna, Thunnus albacares, from Compound-Specific Nitrogen Isotope Analysis of Proteinaceous Amino Acids" in *Stable Isotopes as Indicators of Ecological Change*, T. D. Dawson, R. T. W. Siegwolf, Eds. (Elsevier, 2007), pp. 173–190.

46. F. Melin, GMIS - SeaWiFS Monthly climatology sea surface Chlorophyll-a concentration (9km) in mg.m^-3. *European Commission, Joint Research Centre (JRC)*, [Dataset] (2013).

47. D. J. S. Montagnes, J. A. Berges, P. J. Harrison, F. J. R. Taylor, Estimating carbon, nitrogen, protein, and chlorophyll a from volume in marine phytoplankton. *Limnology and Oceanography* **39**, 1044–1060 (1994).

48. F. Carr, Orthogonal Linear Regression (https://www.mathworks.com/matlabcentral/fileexchange/16800-orthogonal-linear-regression), MATLAB Central File Exchange (2023) (September 25, 2023).

49. B. N. Popp, *et al.*, Effect of phytoplankton cell geometry on carbon isotopic fractionation. *Geochimica et Cosmochimica Acta* **62**, 69–77 (1998).

50. R. R. Bidigare, *et al.*, Variations in the stable carbon isotopic composition of algal biomarkers. *Abstracts, 18th International Meeting on Organic Geochemistry*, 22–26 (1997).

51. E. B. Wilkes, S. J. Carter, A. Pearson, CO2-dependent carbon isotope fractionation in the dinoflagellate Alexandrium tamarense. *Geochimica et Cosmochimica Acta* **212**, 48–61 (2017).

52. S. J. Hurley, B. A. Wing, C. E. Jasper, N. C. Hill, J. C. Cameron, Carbon isotope evidence for the global physiology of Proterozoic cyanobacteria. *Sci. Adv.* **7**, eabc8998 (2021).

53. S. Burkhardt, I. Zondervan, U. Riebesell, Effect of CO2 concentration on C:N:P ratio in marine phytoplankton: A species comparison. *Limnology and Oceanography* **44**, 683–690 (1999).

54. U. Riebesell, S. Burkhardt, A. Dauelsberg, B. Kroon, Carbon isotope fractionation by a marine diatom:dependence on the growth-rate-limiting resource. *Mar. Ecol. Prog. Ser.* **193**, 295–303 (2000).

55. U. Riebesell, A. T. Revill, D. G. Holdsworth, J. K. Volkman, The effects of varying CO2 concentration on lipid composition and carbon isotope fractionation in Emiliania huxleyi. *Geochimica et Cosmochimica Acta* **64**, 4179–4192 (2000).